Acta Oceanol. Sin., 2020, Vol. 39, No. 1, P. 52–62
https://doi.org/10.1007/s13131-019-1466-0
http://www.hyxb.org.cn
E-mail: hyxbe@263.net

The impact of oceanic processes on the transient climate response: a tidal forcing experiment

Yi Yu[1, 3], Hailong Liu[2, 4, 6*], Pengfei Lin[2, 4], Jian Lan[5]

[1] Southern Marine Science and Engineering Guangdong Laboratory (Zhuhai), Zhuhai 510275, China

[2] State Key Laboratory of Numerical Modeling for Atmospheric Sciences and Geophysical Fluid Dynamics, Institute of Atmospheric Physics, Chinese Academy of Sciences, Beijing 100029, China

[3] State Key Laboratory of Satellite Ocean Environment Dynamics, Second Institute of Oceanography, Ministry of Natural Resources, Hangzhou 310012, China

[4] College of Earth Sciences, University of Chinese Academy of Sciences, Beijing 100049, China

[5] College of Oceanic and Atmospheric Sciences, Ocean University of China, Qingdao 266003, China

[6] Center for Ocean Mega-Science, Chinese Academy of Sciences, Qingdao, 266071, China

Received 28 October 2018; accepted 15 April 2019

Abstract

In this study, the impact of oceanic processes on the sensitivity of transient climate change is investigated using two sets of coupled experiments with and without tidal forcing, which are termed Exp_Tide and Exp_Control, respectively. After introducing tidal forcing, the transient climate response (TCR) decreases from 2.32 K to 1.90 K, and the surface air temperature warming at high latitudes decreases by 29%. Large ocean heat uptake efficiency and heat storage can explain the low TCR in Exp_Tide. Approximately 21% more heat is stored in the ocean in Exp_Tide (1.10×10^{24}J) than in Exp_Control (0.91×10^{24}J). Most of the large ocean warming occurs in the upper 1 000 m between 60°S and 60°N, primarily in the Atlantic and Southern Oceans. This ocean warming is closely related to the Atlantic Meridional Overturning Circulation (AMOC). The initial transport at mid- and high latitudes and the decline in the AMOC observed in Exp_Tide are both larger than those observed in Exp_Control. The spatial structures of AMOC are also different with and without tidal forcing in present experiments. The AMOC in Exp_Tide has a large northward extension. We also investigated the relationship between AMOC and TCR suggested by previous studies using the present experiments.

Key words: tidal forcing, transient climate response, ocean heat uptake, Atlantic Meridional Overturning Circulation

Citation: Yu Yi, Liu Hailong, Lin Pengfei, Lan Jian. 2020. The impact of oceanic processes on the transient climate response: a tidal forcing experiment. Acta Oceanologica Sinica, 39(1): 52–62, doi: 10.1007/s13131-019-1466-0

1 Introduction

The equilibrium climate sensitivity (ECS) is defined as the steady-state global mean surface air temperature (SAT) change resulting from a doubling in the concentration of carbon dioxide (e.g., Gregory et al., 2004). It is a fundamental metric for measuring the response of the climate system to greenhouse gases. However, the climate system is never in a steady state, due to changes in both greenhouse gases and heat storage in the ocean (e.g., Levitus et al., 2001). These effects limit the usefulness of the ECS in studying the temporal changes in the climate system. Cubasch et al. (2001) introduced another metric, the transient climate response (TCR), to measure temporal changes in climate sensitivity. The TCR is defined as the global mean SAT change at the time of CO_2 doubling in an idealized 1%/a CO_2 increase experiment (e.g., Cubasch et al., 2001; Randall et al., 2007). Therefore, the TCR is determined not only by radiative heating due to greenhouse gases and climate feedbacks, but also by the ocean heat uptake (OHU).

Large variations are presented in the TCR values estimated from simulations using different climate models in previous studies. Raper et al. (2002) found that TCR values ranged from 1.3 to 2.3°C using models from the Coupled Model Intercomparison Project phase 2 (CMIP2). The ranges for the CMIP3 and CMIP5 models, 1.2–2.4°C (Meehl et al., 2007) and 1.1–2.6°C (Flato et al., 2013), respectively, are similar to those obtained from CMIP2. Kuhlbrodt and Gregory (2012) found that the ratio of the ensemble standard deviation of the TCR to the ensemble mean is approximately 20% for the models from CMIP5. Winton et al. (2014) found that the estimated TCR values are also significantly different even among members of the GFDL model family, the TCR varies from 1.5 to 2.0°C.

By how much and how (that is, through what processes) OHU affects the TCR remain fundamental questions. Raper et al. (2002) estimated that changes in the OHU can lead changes of

Foundation item: The National Key Research and Development Program for Developing Basic Sciences under contract Nos 2016YFC1401401 and 2016YFC1401601; the "Strategic Priority Research Program" of the Chinese Academy of Sciences under contract Nos XDA11010304, XDA05110302 and XDC01040100; the National Natural Science Foundation of China under contract Nos 41576026, 41576025, 41776030 and 41931183.

*Corresponding author, E-mail: lhl@lasg.iap.ac.cn

the TCR in approximately 15% based on the models from CMIP2. We can identify some common model features from this multiple models' comparison, but we cannot closely examine the physical processes involved in the models. Therefore, many studies use experiments that employ the same ocean or atmospheric component and change the other components (Meehl et al., 2004; Winton et al., 2013) or perturb the parameters of the ocean component (Huang et al., 2003; Collins et al., 2007; Brierley et al., 2010). The experiments described by Meehl et al. (2004) and Winton et al. (2013) both show that the effect of the atmospheric component on the TCR seems to be larger than that of the ocean component. The perturbed parameter experiments also show small changes in the TCR values, primarily because other physical processes cancel out this effect (Huang et al., 2003; Collins et al., 2007; Brierley et al., 2010). However, they also found that there are significant (compared to the natural variability) regional variations among the experiments. Moreover, recent studies have shown that the TCR depends on the spatial pattern of OHU (e.g., Rose et al., 2014). Therefore, it is still necessary to understand the uncertainties in OHU and its effect on the TCR in climate models.

There are several oceanic processes that can affect OHU and the TCR. Boé et al. (2009) found that the mixing process in the polar region is closely related to a deep ocean warming in the CMIP models. Griffies et al. (2015) also noted the fundamental role the ocean mesoscale features play in determining the transient OHU. Recently, more studies have focused on the Atlantic Meridional Overturning Circulation (AMOC, Rugenstein et al., 2013; Kostov et al., 2014; Winton et al., 2014), because of its crucial role in determining high latitude climates. This is also the topic that we address in the present study. Rugenstein et al. (2013) found that models that produce large AMOC declines also display less high-latitude warming than models with small AMOC declines. The AMOC decline diminishes the warming by weakening the poleward ocean heat transport and increasing the ocean heat uptake. Kostov et al. (2014) found that the control AMOC is more closely related to surface climate change in the CMIP5 model responses to instantaneous CO_2 quadrupling, because a deeper and stronger AMOC can store more heat at intermediate depths and may delay the surface temperature response. Winton et al. (2014) found that the AMOC behavior, rather than horizontal resolution, produces differences in the TCR in their suite of experiments with different horizontal resolutions. The TCR is found to be closely related to the magnitude of the control climate AMOC and its decline under idealized forcing.

The uncertainty in the decline of the AMOC is significant in present state-of-the-art models. The Intergovernmental Panel on Climate Change Fourth Assessment Report (IPCC AR4) suggested that the AMOC would decline by an amount between 0% and more than 50% in the 21st century, based on coupled model projections (Solomon et al., 2007; Gregory et al., 2005) and the AMOC decrease in 2100 was approximately 20%–30% for the RCP4.5 scenario and 36%–40% for the RCP8.5 scenario in the IPCC AR5 (Weaver et al., 2012; Collins et al., 2013). Reintges et al. (2017) determined that the model uncertainty is the largest contribution to the AMOC projection uncertainty. Munk and Wunsh (1998) pointed out that the winds and tides are the only possible source of mechanical energy to drive ocean thermohaline circulations. The box model simulations also supported this new viewpoint (Huang, 1999; Guan and Huang, 2008; Shen and Guan, 2015). It is estimated that tides can provide 1 TW energy to drive the interior mixing, and the remaining energy comes from winds. In our recent work (Yu et al., 2016), we introduced eight baro-

tropic equilibrium tides into an ocean general circulation model. We also found that the upper cell of the AMOC is significantly changed. Therefore, we will investigate the change in the OHU and the TCR in the coupled model with and without the tidal forcing in the present paper. The purpose of the present study is twofold: to fully understand the role of the tidal processes in the climate system and to understand the behavior of our coupled model when the AMOC changes.

This paper is organized as follows. Section 2 describes the coupled model we used in this paper and the experiment structure. The results, in terms of the effects of tidal forcing on the transient climate change, the OHU and the changes in the AMOC are presented in Section 3. Section 4 contains the concluding remarks and discussion.

2 Model and experimental design

The climate model used in this study is the Flexible Global Ocean-Atmosphere-Land System model, spectral version 2 (FGOALS-s2, Bao et al., 2013, Lin et al., 2013), which was developed by the State Key Laboratory of Numerical Modeling for Atmospheric Sciences and Geophysical Fluid Dynamics of the Institute of Atmospheric Physics (LASG/IAP). The atmospheric and oceanic components of FGOALS-s2 are SAMIL2 (Bao et al., 2010) and the LASG/IAP Climate System Ocean Model version 2 (LICOM 2.0, Liu et al., 2012), respectively. The resolution for SAMIL2 is 2.8°×1.7° in horizontal, and has 26 levels in vertical. A coarse resolution of LICOM2.0 is used here. It has an approximately 1° resolution in horizontal and has 30 vertical levels. The isopycnal and diapycnal mixing in LICOM2.0 are from Gent and Mc Willimas (1990) with the thickness diffusivity of 500 m^2/s and from Canuto et al. (2001). The performance of the low resolution LICOM2.0 has been evaluated by Liu et al. (2012). The biases of LICOM2.0 in terms of water properties and ocean circulation are comparable with those of simulations from the Coordinated Ocean-ice Reference Experiments (COREs, Griffies et al., 2009b).

Yu et al. (2016) implemented tidal forcing into the standalone LICOM 2.0 based on the formula of Griffies et al. (2009a), to investigate the effects of tides on ocean climates. The horizontal gradient term related to the sea surface height (SSH) of the barotropic equation is replaced by the term $\nabla[(1-\alpha)\eta+(1+k-h)\eta_{et}]$, where η is SSH, and η_{et} is the SSH due to the equilibrium tides. The parameter α=0.948 accounts for the modification of the ocean's tidal response as a result of self-attraction and loading (SAL). Variables k and h are Love numbers ($1+k-h=0.7$) that account for the reduction in ocean tides because of the deformation of the solid earth by tidal forcing. Four diurnal (K_1, O_1, P_1, Q_1) and four semi-diurnal (M_2, S_2, N_2, K_2) constituents are considered in the present study, based on Table 13.1 of Griffies et al. (2009a). In addition, in order to efficiently damp the extra tidal energy and obtain a stable solution, a drag term was added to the barotropic equation following Schiller and Fiedler (2007).

In the present study, two sets of coupled experiments are conducted, both with and without tidal forcing (Fig. 1). Each set includes two experiments: a pre-industrial control run and a 143-year 1%/a CO_2 increasing experiment. All the experiments follow CMIP5 protocols (Taylor et al., 2012). The experiments are termed Exp1, 2, Exp_Control, Exp_Tide, respectively, and the two 1%/a CO_2 increasing runs (Exp_Tide and Exp_Control) indicated the presence and absence of tidal forcing, respectively. Notably, Exp 1 and Exp_Control are experiments that we submitted to CMIP5. The two experiments are identical in their setup except for the tides. Exp_Control begins after a long-term (approximately 900 years) spin up integration. The pre-industrial control

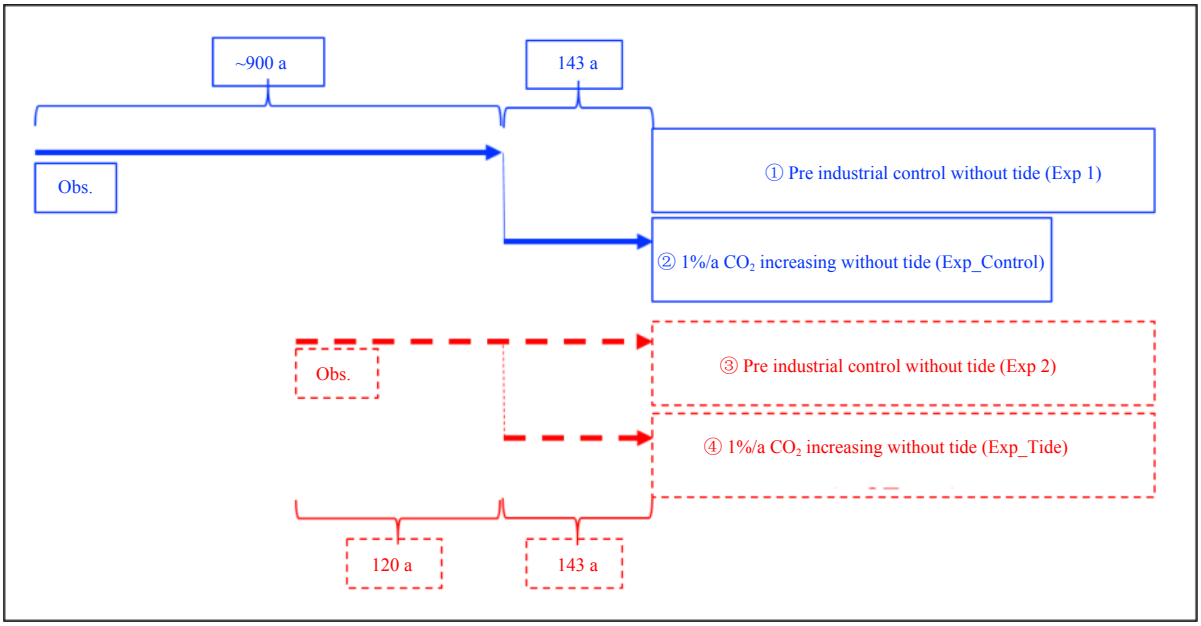

Fig. 1. Experimental design of the present study.

run normally requires a long spin-up, whereas Exp_Tide began from a short spin up (120-year integration). The pre-industrial control run for Exp_Tide remained relatively stable after 100 years, and He et al. (2017) suggested there yields consistent results with 100-year spin-up and 400-year spin-up. Thus, it was appropriate to analyze the impact of tidal forcing on the TCR. The results from the last 143 years of the two pre-industrial control runs, Exp 1 and Exp 2, are used as a reference to compute the temperature changes due to CO_2 increases, that is, the TCR. The linear trend from the last 143 years of the two pre-industrial control runs was computed and deducted from the results of Exp_Control and Exp_Tide.

After introducing the tidal forcing, the barotropic circulation was reduced, especially in the coastal regions (Yu et al., 2016). The transport of AMOC was also found to have diminished significantly, whereas the transport by the Antarctic Bottom Water was slightly enhanced. The changes in circulation were all related to increases in the bottom friction and the vertical viscosity due to tidal forcing. The transport by the upper cell of the AMOC also decreased south of 35°N, which is similar to the results of Yu et al. (2016). However, the transport was slightly enhanced north of 35°N in the coupled experiment with tidal forcing. This may be related to complex physical processes involving the coupling with both the atmosphere and the sea ice. In the present study, we do not focus on explaining why the AMOC was enhanced in Exp_Tide. Instead, we focus on the relationship between the AMOC and the OHU or the TCR.

3 Results

3.1 *Transient climate response to CO_2 increase*

Figure 2 presents the global annual SAT changes under 1% CO_2 increases in the two experiments. The change in SAT depicts an approximately linear trend in Exp_Control. However, when tidal forcing is included, the SAT responses exhibit some non-linearity under CO_2 increases. There is no significant surface warming in the first 30 years, and then the slope of the surface warming is larger than in the control experiment. This non-linearity

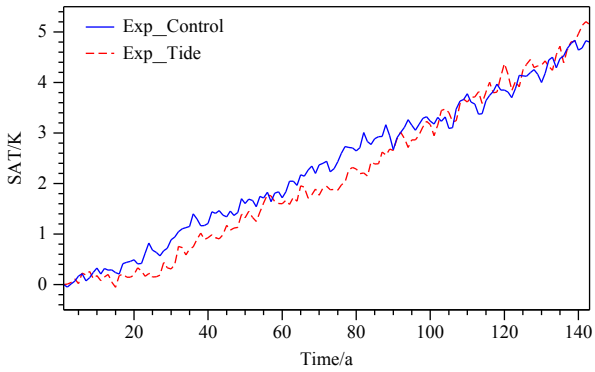

Fig. 2. Global mean surface air temperature (SAT) changes for Exp_Control (blue) and Exp_Tide (red) in 1%/a CO_2 increasing experiments.

phenomenon is also exhibited by other climate models (e.g., Winton et al., 2013). The non-linear behavior may depend on the evolution of the ocean mixing layer and the pattern of SST (Winton et al., 2010) and changes in the state of the deep ocean (e.g., Held et al., 2010). The TCR, which is defined as the 20-year (years 61-80) average global mean SAT change at the time of CO_2 doubling, is an often-used measure of the magnitude of climate sensitivity. The ensemble mean of the TCR in IPCC models is 1.8 K± 0.37 K for AR4 (Winton et al., 2010) and 1.8 K±0.6 K for AR5 (Flato et al. 2013). The TCR for Exp_Control and Exp_Tide are 2.32 K and 1.90 K, respectively (Table 1). The value of TCR with and without tidal forcing is located within the range of multi-model values. Therefore, we supposed that the model simulations in our study are believable. The difference of TCR between Exp_Tide and Exp_Control in the present study is 0.42 K, which is comparable to the multi-model standard deviation of AR4 (0.37 K) and AR5 (0.60 K). Therefore, tides have significant influence on the projection of transient surface warming in our study. The approximately 19% smaller TCR in Exp_Tide suggests that tidal forcing can temporarily suppress surface air temperature warming. To

Table 1. Key metrics for the Exp_Control and the Exp_Tide experiments

	Exp_Control	Exp_Tide
TCR/K	2.32	1.90
Ocean heat uptake efficiency/W·m^{-2}·K^{-1}	0.49	0.63
Ocean heat storage change/10^{24} J·PW^{-1}	0.91/0.41	1.10/0.50
Depth of 80% heat change/m	580	700

minimize the impact of the non-linear behavior observed in Exp_Tide, the TCR can be calculated using the 143-year average of surface air temperature change (Winton et al., 2013). With this method, the value of the TCR in Exp_Tide is 2.14 K. This value is higher than the TCR calculated from the average global mean SAT changes in years 61–80, but still lower than that for Exp_Control.

As CO_2 continues to increase, the change in SAT in the two experiments decreases. At the time of CO_2 quadrupling, the 20-year average SAT is 4.57 K for Exp_Tide, slightly larger than that for Exp_Control (4.43 K). We noted that the ratio of the difference of SAT change between two experiments to their average is approximately 20% at the time of CO_2 doubling, approximately six times the value at the time of CO_2 quadrupling. This result suggests that the impact of tidal forcing on surface warming is significant at the time of CO_2 doubling, whereas the atmospheric component plays the main role in climate sensitivity, rather than the ocean component, over longer time scales when CO_2 quadruples (Meehl et al., 2004). Based on these results, we concentrated on the impact of tidal forcing at the time of CO_2 doubling.

The SAT anomaly is asymmetrical between two hemispheres, especially at high latitudes. There is a larger SAT anomaly at northern high latitudes than in southern high latitudes (Fig. 3), as is projected by most coupled models (e.g., Bitz et al., 2006). The Arctic polar amplification leads to the larger simulated surface warming at the northern high latitudes (Holland and Bitz 2003). At the time of CO_2 doubling, the surface warming north of 45°N is 4.43 K in Exp_Control, whereas it is only 3.12 K after introducing the tidal forcing, corresponding to a reduction of approximately 30% (Table 2). The maximum surface warming for Exp_Control is 8.62 K, which is approximately 3 K higher than that seen in Exp_Tide (Fig. 3). The surface warming is relatively weaker in the southern high latitudes than that in the northern high latitudes. This phenomenon is typically attributed to the strong ocean heat uptake in the Southern Ocean (e.g., Gregory, 2000; Exarchou et al. 2014). At the time of CO_2 doubling, the surface warming south of 45°S is 1.70 K for Exp_Control, whereas it is 1.24 K for Exp_Tide after the tidal forcing is introduced (Table 2). Although the change is smaller than that at the northern high latitudes, the ratio of the changes in the two hemispheres is similar to each other; the reduction is 27% in the Southern Hemisphere. In contrast to the maximum surface warming, the minimum surface warming for Exp_Tide (0.5 6 K) is similar to the value for Exp_Control (0.72 K). The changes in SAT between 45°N and 45°S are 2.06 K for Exp_Control and 1.80 K for Exp_Tide, which are smaller than

Table 2. Changes in area mean surface air temperature (SAT, K) over three latitudinal bands for Exp_Control and Exp_Tide

	Surface air temperature/K	
	Exp_Control	Exp_Tide
North of 45°N	4.43	3.12
45°N–45°S	2.06	1.80
South of 45°S	1.70	1.24

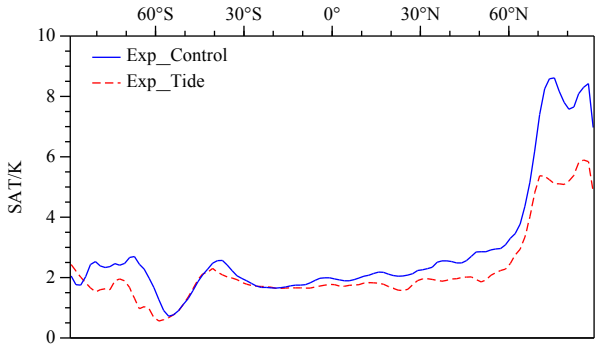

Fig. 3. Zonal mean surface air temperature (SAT) changes when CO_2 is doubled (during years 61–80) for Exp_Control (blue) and Exp_Tide (red).

those observed at the northern high latitudes and larger than those observed at southern high latitudes, respectively. However, the reduction due to tidal forcing is only approximately 13%, less than half the value at high latitudes. This result reveals that the tidal forcing affects not only the transient climate response but also regional climate changes in response to CO_2 increases.

Figure 4 shows the geographic pattern of SAT changes in the two experiments. Both experiments reflect the typical pattern of SAT change that can be seen in almost all climate models. The largest surface warming occurs at northern high latitudes, and minimal warming, even cooling, is found in the North Atlantic and the Southern Ocean (Fig. 4). However, when the tidal forcing is included in the climate model, there are significant regional differences in the geographic patterns of SAT change between the two experiments. At the time of CO_2 doubling, the simulated warming in Exp_Tide in the Arctic is 5.73 K, lower than that of Exp_Control (8.92 K). The maximum Artic warming is located in the Barents Sea for Exp_Control, whereas it is located in the Norwegian Sea for Exp_Tide. A cooling area is present in the North Atlantic in both experiments. A reduction in meridional heat transport may create the cooling area (Rugenstein et al. 2013). The latitudinal band of the cooling center is approximately 45°–70°N for Exp_Tide, which is larger than the latitude band for Exp_Control (45°–55°N). Moreover, there is an additional cooling region in the northern portion of the Ross Sea in Exp_Tide with a 3.44 K cooling of the SAT. Both the initial SAT and TCR with tides are smaller at northern high latitudes (Figs 4c, d). This result seems to reveal the simulation of TCR is related to the simulation of the initial state. Recently, He et al. (2017) investigated the differences in TCR between two different base climates, a preindustrial and a present-day climate. They found that the experiment from the present-day climate has a much larger TCR than that from the preindustrial climate. The behavior of two experiments in the present study is similar to He et al. (2017).

In general, after introducing the tidal forcing, we found that the TCR is reduced from 2.32 K to 1.90 K. Large reductions in SAT occur within the high latitude regions of both hemispheres with a ratio of approximately 30%, whereas the change in SAT between 45°N and 45°S is small (only ~13%). This result indicates that the differences between the high and low latitudes in Exp_Tide with tidal forcing decrease.

3.2 *Response in ocean heat uptake*

To understand the relationship between the TCR and oceanic processes in the present study, we investigate the change in

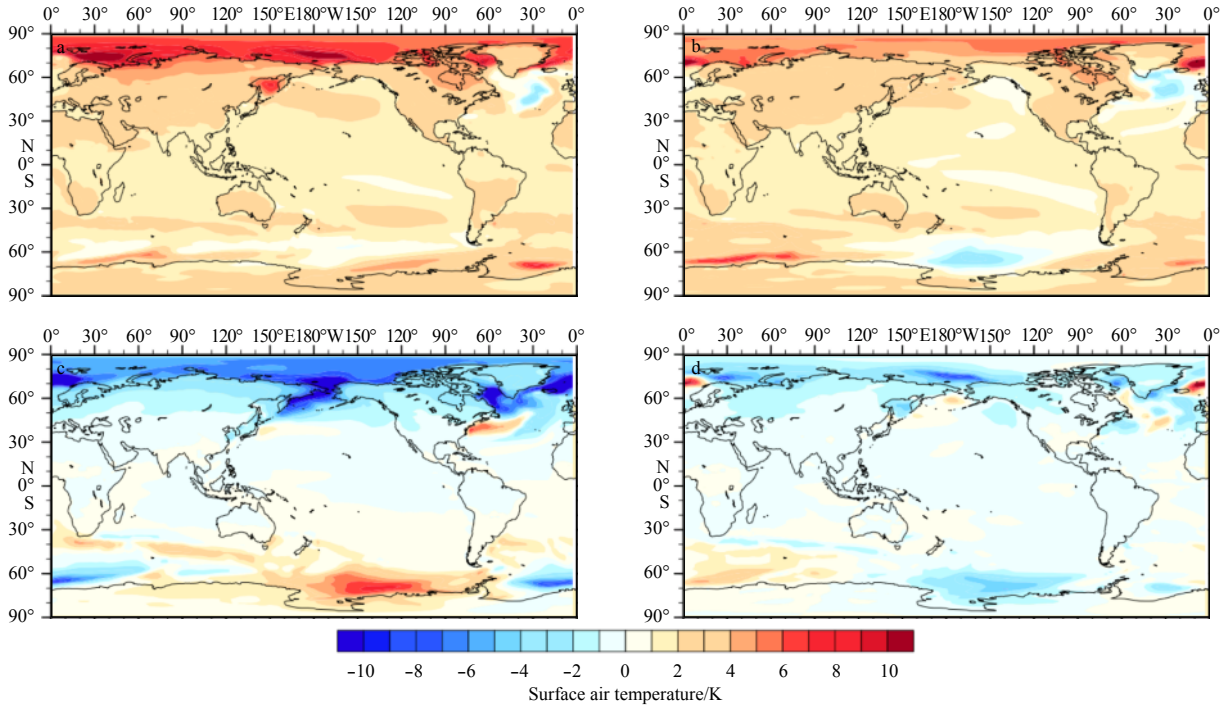

Fig. 4. Surface air temperature (SAT) changes when CO_2 is doubled (during years 61–80) for Exp_Control (a) and Exp_Tide (b), the difference between the two experiments (Exp_Tide minus Exp_Control) at the beginning (c) and the difference of SAT change (Exp_Tide minus Exp_Control) (d), unit: K.

OHU between the two sets of experiments. The SAT change in response to radiative forcing is determined by the heat balance between the net radiative flux at the top of the atmosphere (TOA), denoted as N hereafter, and the radiative heating due to greenhouse gases (e.g., Gregory et al., 2004), denoted as F hereafter. This relationship can be written as follows:

$$N = F - \alpha \Delta T, \tag{1}$$

where ΔT is the SAT change and α is the climate feedback parameter. Gregory and Forster (2008) further suggested that the climate system has absorbed approximately all the heat in the ocean. Therefore, N can be expressed as $N \approx \kappa \Delta T$, in which κ is the ocean heat uptake efficiency coefficient. The ocean heat uptake efficiency coefficient can be calculated by performing a linear regression between the net heat flux, N, and the SAT change (e.g., Exarchou et al., 2014). Substituting N into Eq. (1), we obtain a relationship between the TCR and κ as follows: $\Delta T = \dfrac{F}{\alpha + \kappa}$. Based on this expression, we find that the TCR is determined by the radiative forcing, ocean heat uptake efficiency and the climate sensitivity parameter. The faster the heat is transported downwards into the ocean will lead to a larger ocean heat efficiency value and thus reduced surface warming.

In the present study, the ocean heat uptake efficiency coefficient, κ, is 0.49 W/(m²·K) for Exp_Control and 0.63 W/(m²·K) for Exp_Tide (Fig. 5 and Table 1). In Exp_Tide, κ is approximately 28% higher than that of Exp_Control (Table 1). We also calculated the ocean heat storage change (Table 1). Approximately 21% more heat is stored in the ocean in Exp_Tide (1.10×10^{24}J) than in Exp_Control (0.91×10^{24}J). The high ocean heat uptake efficiency and heat storage can explain the low TCR in Exp_Tide.

The simulated OHU at the time of doubling of CO_2 for the entire water column, the upper 1 000 m and below 1 000 m are shown in Figure 6. The OHU is defined as $\int_{-H}^{0} c\Delta T_{\text{ocean}} \mathrm{d}z$, where c [$=4.1\times10^6$ /(Jm³·K)] is the volumetric heat capacity, and ΔT_{ocean} is the ocean temperature change. The global mean values confirm that much more of the heating in Exp_Tide (approximately 90%) occurs in the upper 1 000 m. This outcome leads to a larger OHU efficiency and a smaller SAT for Exp_Tide. Moreover, this large upper-layer heating can be found in the Pacific-Indian

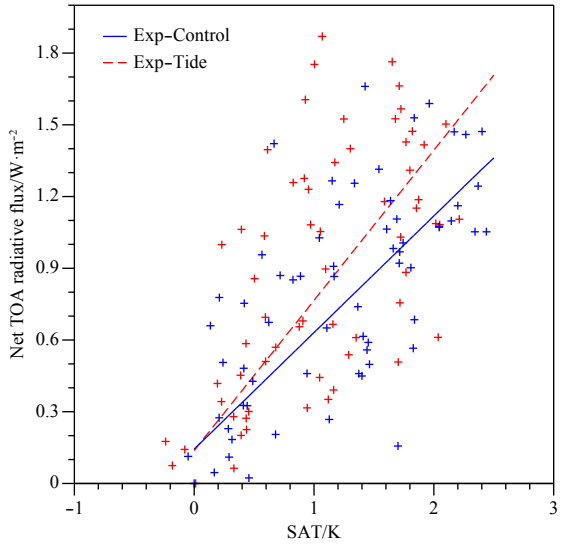

Fig. 5. Scatter plot showing changes in surface air temperature (SAT, K) and the net radiation flux at the top of the atmosphere (TOA, W/m²) for Exp_Control (blue) and Exp_Tide (red). The lines are linear regressions based on the two experiments.

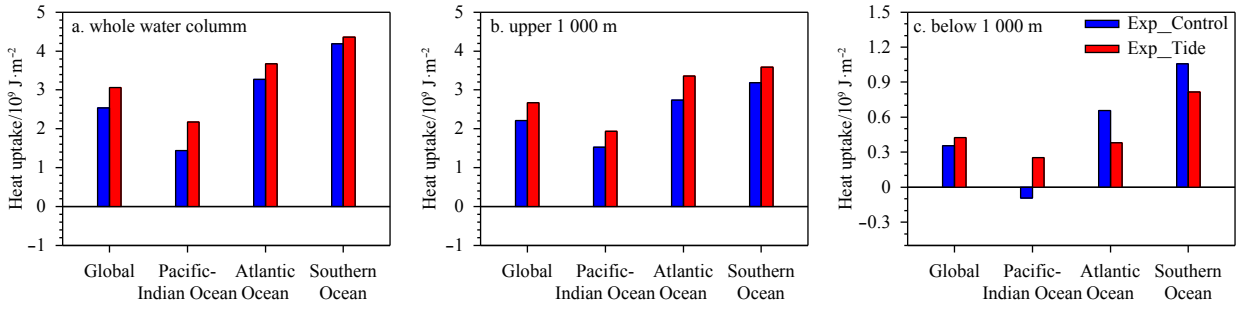

Fig. 6. The ocean heat uptake (10^9 J/m^2) for the whole water column (a) , the upper 1 000 m (b) and the portion below 1 000 m (c) for Exp_Control (blue) and Exp_Tide (red).

Ocean, the Atlantic Ocean (including the Arctic Ocean) and the Southern Ocean. Interestingly, although the global value of OHU below 1000 m for Exp_Tide is larger than that for Exp_Control, the heating in the Atlantic and the Southern Ocean is smaller. That is, the large deep ocean heat uptake seen in Exp_Tide primarily occurs in the Pacific Ocean (Fig. 6).

The spatial distribution of the warming can be better represented in terms of zonal mean ocean warmings in the two experiments (Fig. 7), in which the upper 1 000 m has been magnified. At the time of CO_2 doubling, the most notable difference between the two experiments occurs in the Arctic Ocean, where the temperature for Exp_Tide is approximately 1 K colder than that observed in Exp_Control. The warming in Exp_Tide primarily occurs between 60°S and 60°N, which can be clearly observed in the figure presenting the difference (Fig. 7c). Warming centers with a magnitude of 0.5 K appear in the upper 1 000 m. The SST in Exp_Tide are cooler than those seen in Exp_Control, which tends to cause more heat to enter into the ocean in Exp_Tide. Examining the warming in separate basins, we find that the warming is centered at depths of approximately 100–200 m in the tropical region of the Pacific-Indian Ocean, while the warming occurs at depths of 500–1 000 m in the Atlantic Ocean and the Southern Ocean (not shown). The different of warming in the ocean basin maybe associated with the meridional overturning circulation. The AMOC in the Atlantic Ocean and Deacon Cell in the Southern Ocean can drive the warm water into the deep ocean. In opposite to the AMOC and Deacon Cell, the meridional overturning circulation is absent in Pacific-Indian Ocean. Thus, the warming centers in the Atlantic and Southern Oceans are deeper than that in the Pacific-Indian Ocean. Noted that, the Antarctic Bottom Water (AABW) is weaker in Exp_Tide at the CO_2 doubled (Fig. 9f). Less cool water can transport into the bottom in Exp_Tide. Thus, there exists a warmer signal at the bottom in Exp_Tide (Fig. 7c).

The changes in the vertical integrated ocean heat storage for Exp_Control and Exp_Tide were also investigated in this study. We find that the large warming for Exp_Tide occurs primarily in the Atlantic and Southern Oceans (Fig. 8b). The large warmings

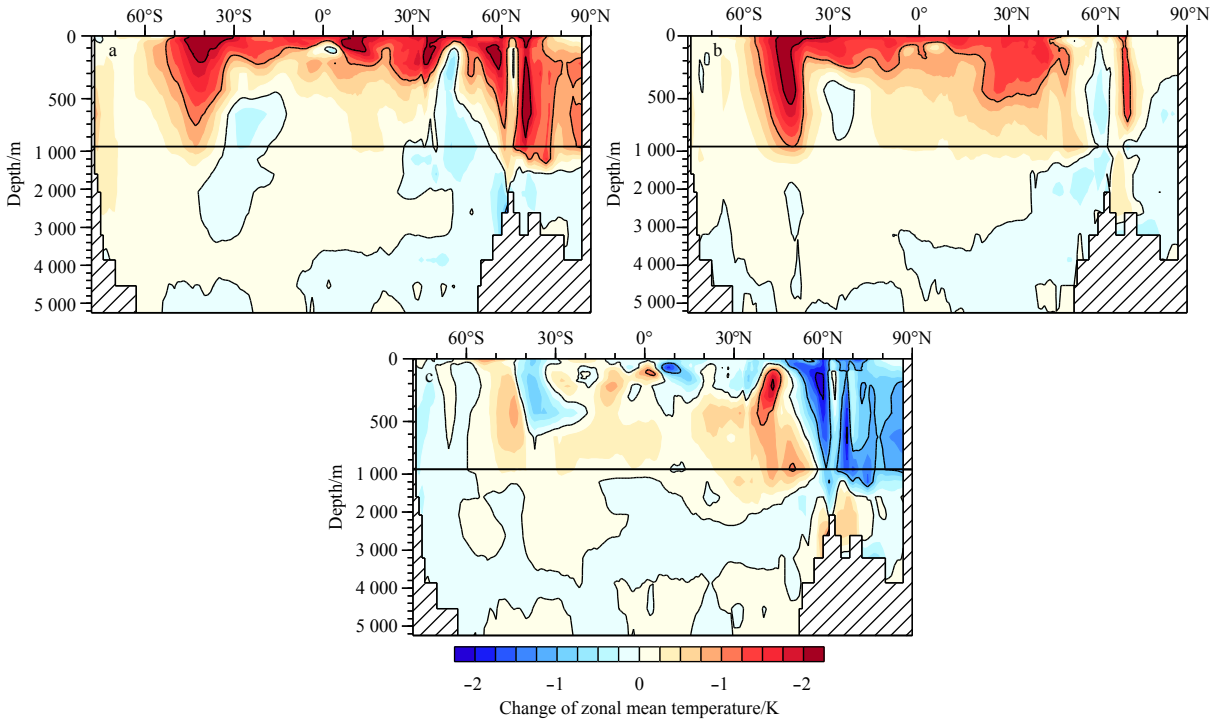

Fig. 7. Changes in zonal mean ocean temperature (K) for Exp_Control (a), Exp_Tide (b) and the difference between the two experiments (Exp_Tide minus Exp_Control) (c), unit:K .

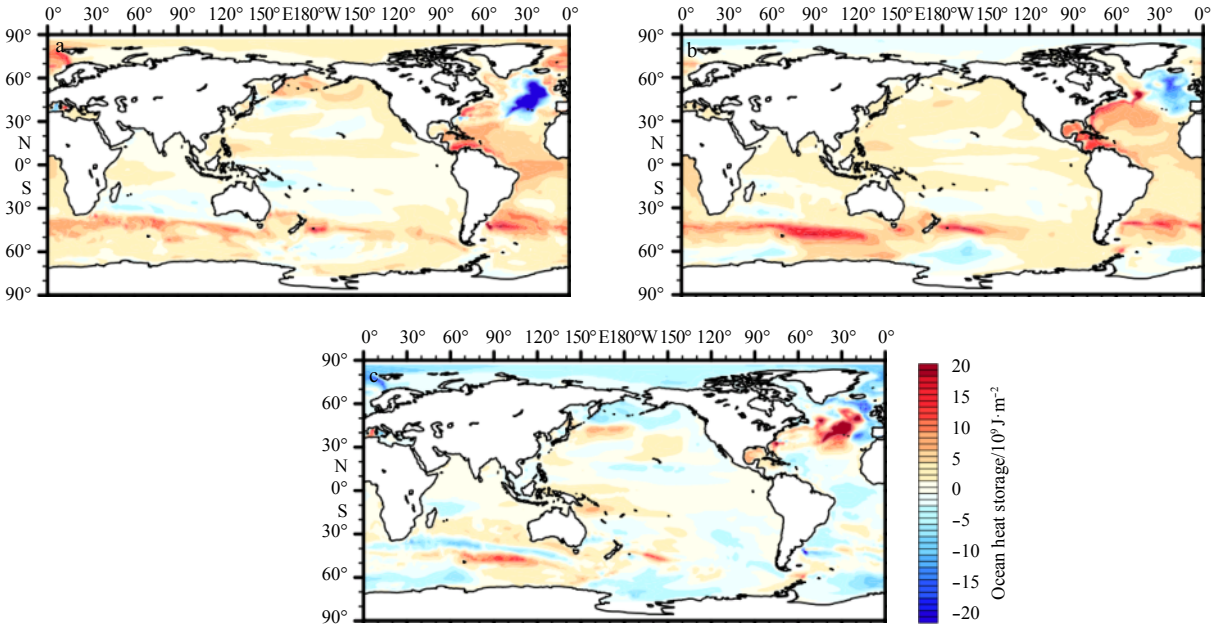

Fig. 8. Change in the vertically integrated ocean heat storage (10^9 J/m^2) for Exp_Control (a), Exp_Tide (b) and the difference between the two experiments (Exp_Tide minus Exp_Control) (c).

appear along the western boundary of the Atlantic Ocean from 10°S to approximately 50°S and along the Antarctic Circumpolar Current (ACC). As in previous studies, the former may be associated with the decline of the AMOC (Winton et al., 2013), and the latter may be caused by the reduction of the convection (Huang et al., 2003) and related to the wind response with an increase in westerlies (figure not shown). In addition to the warming anomalies, there is a notable and large cooling center in the northeastern part of the Atlantic Ocean that has a minimum value of –19.3 GJ/m^2. However, its magnitude has been reduced to approximately half in Exp_Tide.

As shown above, the large OHU leads to a small TCR at the time of doubling of CO_2 in the experiment with tidal forcing. Most of the warming can be found in the upper 1 000 m between 60°S and 60°N, mainly in the Atlantic and Southern Oceans. The larger warming along the western boundary and the reduced cooling between 30°–60°N in the Atlantic Ocean suggest that the AMOC may play an important role. Therefore, in the following section, we investigate the relationship between OHU or the TCR on the one hand and the magnitude of the AMOC or the change in the AMOC on the other hand.

3.3 *The Atlantic Meridional Overturning Circulation*

The relationship between the AMOC at the beginning (year 1) and the changes of AMOC at the CO_2 doubling (years 61–80) of the integration for both Exp_Control and Exp_Tide are investigated. The difference between the two experiments at the beginning and the CO_2 doubling are also shown. In general, Exp_Tide appears as a slightly deeper upper cell of the AMOC than that observed in Exp_Control at both the beginning and the CO_2 doubled (Fig. 9). The structures of AMOC are different in the two experiments, especially in the mid- and high latitudes. The maximum transport fluxes of North Atlantic Deep Water (NADW) for the two experiments south of 40°N at the beginning of the integrations are approximately (16–19)×10^6 m^3/s and are comparable to each other (Table 3). However, the magnitude of the NADW for the Exp_Control begins to reduce quickly poleward of 40°N, measuring only 4.1×10^6 m^3/s for Exp_Control at 50°N, but still 14.2×10^6 m^3/s for Exp_Tide (Table 3). This result suggests that more water is transported in the upper cell of the AMOC in Exp_Tide than in Exp_Control at the initial state.

$D_{80\%}$ is defined as the depth above which 80% of the total global heat storage change occurs, and a larger $D_{80\%}$ is associated with stronger AMOC as CO_2 increasing (Kostov et al., 2014). In the present study, $D_{80\%}$ is approximately 120 m (20%) deeper after introducing the tidal forcing (Table 1). That is, the heating in Exp_Tide primarily occurs in the deeper ocean. In our study, the relationship between $D_{80\%}$ and the magnitude of AMOC, which is defined as the maximum transport at 40°N, agrees with that identified by Kostov et al. (2014).

As CO_2 increases, the magnitude of the AMOC also gradually decreases. The change in the magnitude of the AMOC for Exp_Tide is also larger than that seen in Exp_Control, especially northward of 40°N (Figs 9b and d, Table 3). The average values by which the AMOC decreases are 5.0×10^6 m^3/s and 8.3Sv for Exp_Control and Exp_Tide, respectively, and this decrease is approximately 66% larger for Exp_Tide than that seen in Exp_Control. This result is the same as that described by Winton et.al (2014), who found that larger AMOC declines are associated with larger ocean heat uptake efficiency in a 10-model suite. Winton et al. (2014) also proposed a more complex mechanism by which the AMOC affects the TCR. They suggested that the smaller partitioning of water in the Northern Hemisphere leads to large warming in the North Hemisphere. Therefore, a decrease in the AMOC retards the warming. The differences in AMOC change in two experiments are opposite the differences of AMOC at the beginning, which is also supported by He et al. (2017).

To further understand the relationship between the AMOC and the OHU in the Atlantic Ocean, we compute the Meridional Heat Transport (MHT) for the two experiments during both the first year and years 61–80 (Fig. 10). In general, the MHTs for Exp_Tide during the two periods are smaller than those seen in Exp_Control at almost all latitudes, except between 20°N and 40°N. Although the MHT values at 30°S for Exp_Tide are smaller

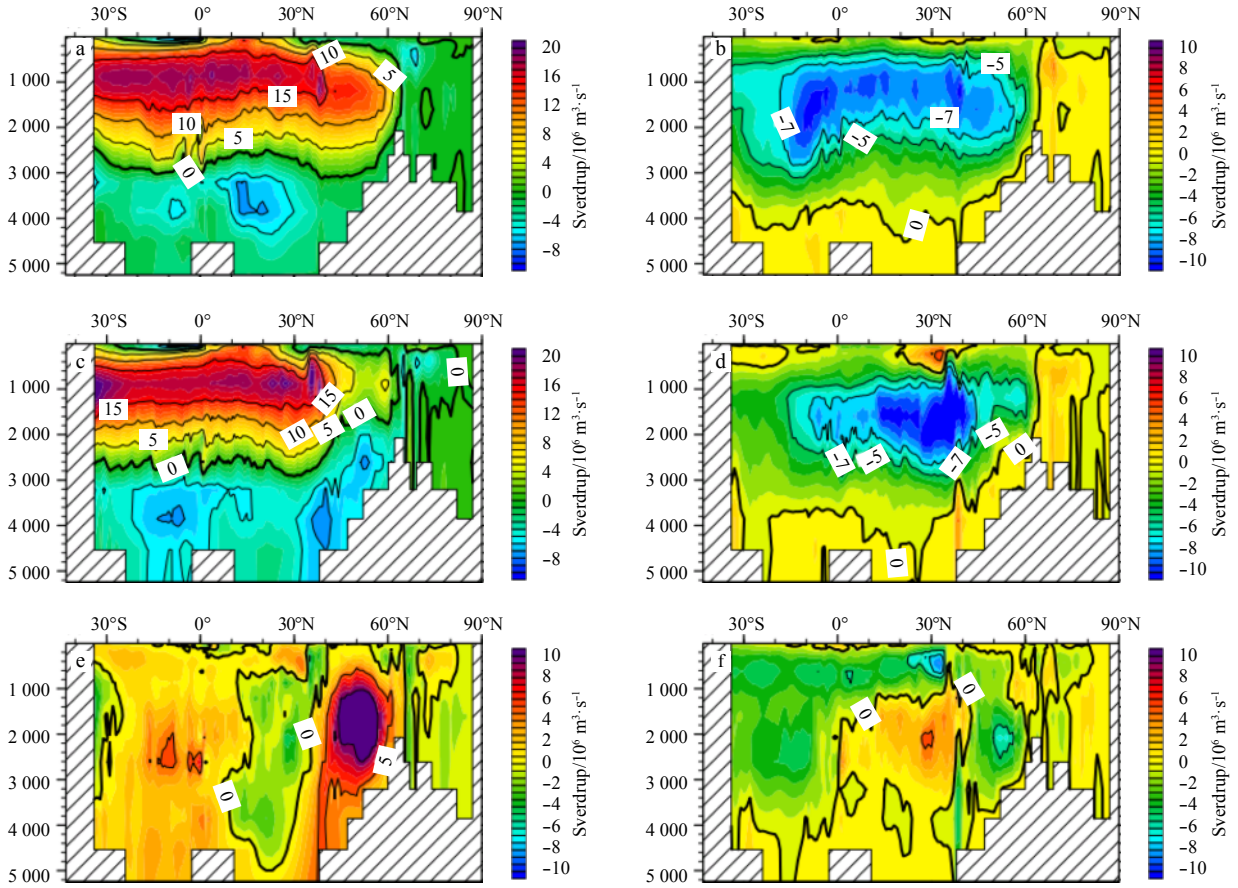

Fig. 9. The Atlantic Meridional Overturning Circulation (AMOC) at the beginning (year 1) (a), the changes at the end (years 61–80) of Exp_Tide (b). (c) and (d) are the same as (a) and (c), but for Exp_Control. (e) and (f) are the different between Exp_Tide and Exp_Control at the beginning and at CO_2 doubling of the experiments (Exp_Tide minus Exp_Control), unit:10^6 m^3/s.

Table 3. The maximum value and change of the AMOC at specific latitudes

	North latitude/(°)	Exp_Control	Exp_Tide
Maximum AMOC/10^6 $m^3 \cdot s^{-1}$	10	18.6	18.8
	20	18.5	17.4
	30	18.8	16.8
	40	14.2	16.7
	50	4.1	14.2
Change of AMOC/10^6 $m^3 \cdot s^{-1}$	10	–4.5	–8.5
	20	–5.1	–7.6
	30	–4.0	–7.9
	40	–6.8	–9.6
	50	–4.4	–7.9
	mean	–5.0	–8.3

than those seen in Exp_Control, the heat storage rate in Exp_Tide (0.14 PW) is still larger than that of Exp_Control (0.12 PW). This result occurs because large amounts of heat are released into the atmosphere in Exp_Control.

Summarized above, more heat was stored into the ocean (Table 1), and the initial AMOC and AMOC decline were larger with tidal forcing. Thus, we supposed that the larger initial AMOC and AMOC decline are associated with larger OHU. We also investigated the mechanism of their relationship. The AMOC declines can weaken poleward ocean heat transport. The larger AMOC declines in Exp_Tide induce less poleward ocean heat transport (Figs 9 and 10). Less poleward ocean heat transport (larger AMOC declines) with tidal forcing made the cooler SST in high latitudes. The cold SST in Exp_Tide lead less ocean heat flux to release (Fig. 6). This process can store more heat into the ocean.

We also found that the MHTs generally decrease with increasing CO_2 at approximately all latitudes. However, the MHTs south of 15°S in both runs increase slightly with increasing CO_2. At 30°S, this increase is from 0.27 PW to 0.29 PW and from 0.07 PW to 0.17 PW for Exp_Control and Exp_Tide, respectively. This result is mainly due to the increasing vertical gradient of temperature in the two experiments. Although the decline in the AMOC is smaller in Exp_Control, the decrease in MHT seen in Exp_Control (0.17 PW) at the equator is larger than that of Exp_Tide (0.1 PW). In other word, a larger decline in volume transport does not guarantee a larger decline in the heat transport. Therefore, the mechanism proposed by Winton et al. (2014) may be model dependent and requires more investigation.

In general, the results from these two sets of experiments follow the conclusions drawn by previous studies: larger values of an initial transport at mid- and high latitudes and declines in the AMOC lead to larger OHU and smaller TCR values (Kostov et al., 2014; Winton et al., 2014). However, investigation of the underlying mechanism reveals that this mechanism maybe model dependent. The differences are predominantly caused by the structure of the AMOC and the location of the heat stored in the up-

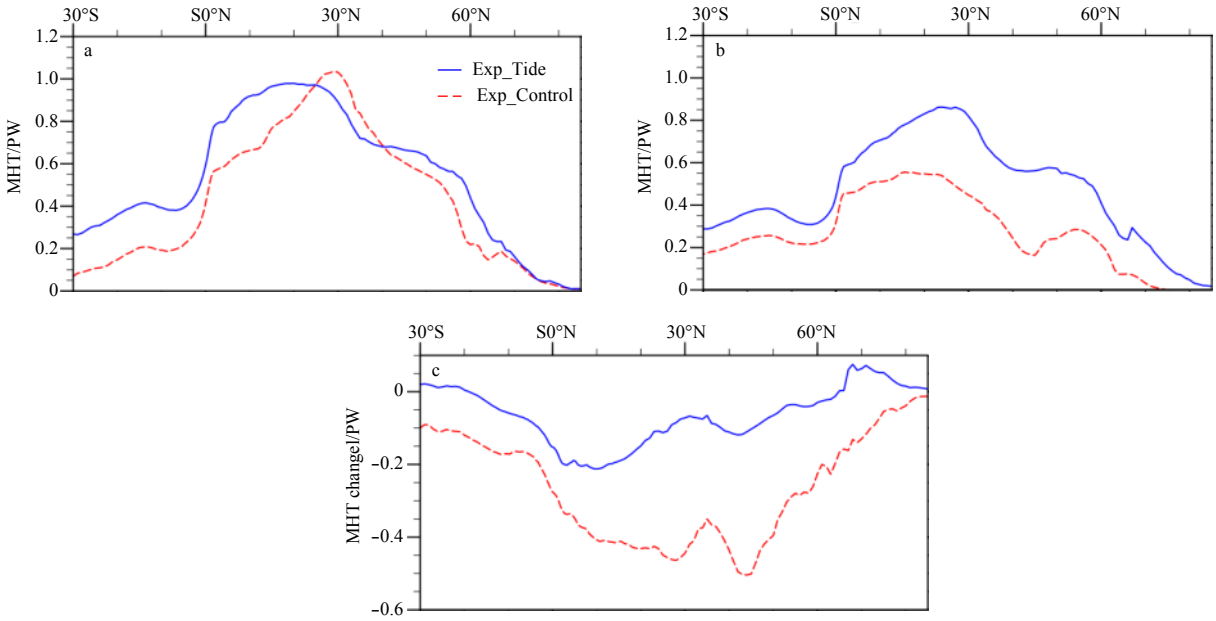

Fig. 10. The Atlantic Meridional Heat Transport (MHT, PW) at the beginning (year 1) (a) and the end (years 61–80) (b), the changes of MHT (c) for Exp_Control (blue) and Exp_Tide (red) .

per ocean.

4 Concluding remarks and discussion

In the present study, the impact of tidal forcing on the sensitivity of transient climate change is investigated using two sets of experiments with and without tidal forcing in a coupled climate model. After introducing the tidal forcing, we found that the TCR is reduced from 2.32 K to 1.90 K. Large reductions in SAT (by approximately 30%) occur in the high latitude regions of both hemispheres, whereas the change in SAT between 45°N and 45°S is small (13%). The ocean heat uptake efficiency coefficient for Exp_Control is smaller than that for Exp_Tide, leading to approximately 21% more heat storage in the ocean in Exp_Tide (1.10×10^{24} J) than in Exp_Control (0.91×10^{24} J). The high ocean heat uptake efficiency and heat storage can explain the low TCR in Exp_Tide. Most of the large warming can be found in the upper 1000 m between 60°S and 60°N, primarily in the Atlantic and Southern Oceans. This warming is closely related to the AMOC. The initial transport at mid- and high latitudes and the decline in the AMOC seen in Exp_Tide are both larger than in Exp_Control. As in previous studies, these two features lead to slowed warming in Exp_Tide.

We also investigated the mechanisms suggested by previous studies, particularly Kostov et al. (2014) and Winton et al. (2014), using the present experiments. Some hypothesizes are similar to previous studies. In our study, large control AMOC has a strong correlation with a large AMOC decline, as suggested by Winton et al. (2014). There is a strong positive correlation between the maximum transport of AMOC and $D_{80\%}$, and Kostov et al. (2014) obtained the same results. However, the spatial structures of the AMOC are different with and without tidal forcing. The AMOC in Exp_Tide has a large northward extension and does not become deeper, as suggested by Kostov et al. (2014). Furthermore, we also found that a larger decline in the volume transport does not guarantee a larger decline in heat transport in the present experiments, as is the case in Winton et al. (2014). This result is due to the changes in the vertical temperature gradient. Based on our results, the mechanism by which the AMOC affects the TCR is model dependent or definition dependent. Therefore, the mechanism by which the AMOC affects the OHU and the TCR is still an open question and needs more investigation using different models.

Interestingly, we also found that the spatial distribution of heat storage may lead to different climate responses and thereby different TCR values. In the present study, the heat is stored predominantly in the upper 1 000 m between 60°S and 60°N in Exp_Tide, whereas it is stored in the Arctic Ocean in Exp_Control. The local feedback between the solar radiation and the sea ice may amplify the warming in the Arctic region and thus increase the SAT. Rose et al. (2014) investigated the effects of the spatial distribution of heat sinks on transient climate responses using a set of aqua-planet experiments. However, they found that high latitude warming leads to large cooling. The differences may be caused by the different experiments conducted. However, these differences require further investigation.

In our study, the two numerical experiments have a different initial state and AMOC structures with CO_2 increasing due to tidal forcing. And the simulation of TCR is sensitive to the differences of the initial state (Figs 4c and d) and AMOC changes (Fig. 9). How to quantify the influence of the initial state and AMOC change on the TCR is a challenging job. We believe that the relationship among them (the AMOC, initial state and TCR) is model dependent and should be investigated further.

References

Bao Qing, Lin Pengfei, Zhou Tianjun, et al. 2013. The flexible global ocean-atmosphere-land system model, spectral version 2: FGOALS-s2. Advances in Atmospheric Sciences, 30(3): 561–576, doi: 10.1007/s00376-012-2113-9

Bao Qing, Wu Guoxiong, Liu Yimin, et al. 2010. An introduction to the coupled model FGOALS1.1-s and its performance in East Asia. Advances in Atmospheric Sciences, 27(5): 1131–1142, doi: 10.1007/s00376-010-9177-1

Bitz C M, Gent P R, Woodgate R A, et al. 2006. The influence of sea ice on ocean heat uptake in response to increasing CO_2. Journal of

Climate, 19(11): 2437–2450, doi: 10.1175/JCLI3756.1
Boé J, Hall A, Qu X. 2009. Deep ocean heat uptake as a major source of spread in transient climate change simulations. Geophysical Research Letters, 36(22): L22701, doi: 10.1029/2009GL040845
Brierley C M, Collins M, Thorpe A J. 2010. The impact of perturbations to ocean-model parameters on climate and climate change in a coupled model. Climate Dynamics, 34(2–3): 325–343, doi: 10.1007/s00382-008-0486-3
Canuto V M, Howard A, Cheng Y, et al. 2001. Ocean turbulence. Part I: One-point closure model-momentum and heat vertical diffusivities. Journal of Physical Oceanography, 31(6): 1413–1426, doi: 10.1175/1520-0485(2001)031<1413:OTPIOP>2.0.CO;2
Collins M, Brierley C M, MacVean M, et al. 2007. The sensitivity of the rate of transient climate change to ocean physics perturbations. Journal of Climate, 20(10): 2315–2320, doi: 10.1175/JCLI4116.1
Collins M, Knutti R, Arblaster J, et al. 2013. Long-term climate change: projections, commitments, and irreversibility. In: Stocker T F, Qin D, Plattner G K, et al, eds. Climate Change 2013: The Physical Science Basis. Contribution of Working Group I to the Fifth Assessment Report of the Intergovernmental Panel on Climate Change. Cambridge, UK and New York, USA: Cambridge University Press.
Cubasch U, Meehl G A, Boer G J, et al. 2001. Projections of future climate change. In: Houghton J T, Ding Y, Griggs D J, et al, eds. Contribution of Working Group I to the Third Assessment Report of the Intergovernmental Panel. London: Cambridge University Press, 526–582.
Exarchou E, Von Storch J S, Jungclaus J H. 2014. Sensitivity of transient climate change to tidal mixing: Southern Ocean heat uptake in climate change experiments performed with ECHAM5/MPIOM. Climate Dynamics, 42(7–8): 1755–1773, doi: 10.1007/s00382-013-1776-y
Flato G, Marotzke J, Abiodun B, et al. 2013. Evaluation of climate models. In: Stocker T F, Qin D W, Plattner G K, et al, eds. Climate Change 2013: The Physical Science Basis. Contribution of Working Group I to the Fifth Assessment Report of the Intergovernmental Panel on Climate Change. Cambridge: Cambridge University Press.
Gent P R, McWilliams J C. 1990. Isopycnal mixing in ocean circulation models. Journal of Physical Oceanography, 20(1): 150–160, doi: 10.1175/1520-0485(1990)020<0150:IMIOCM>2.0.CO;2
Gregory J M. 2000. Vertical heat transports in the ocean and their effect on time-dependent climate change. Climate Dynamics, 16(7): 501–515, doi: 10.1007/s003820000059
Gregory J M, Dixon K W, Stouffer R J, et al. 2005. A model intercomparison of changes in the Atlantic thermohaline circulation in response to increasing atmospheric CO_2 concentration. Geophysical Research Letters, 32(12): L12703
Gregory J M, Forster P M. 2008. Transient climate response estimated from radiative forcing and observed temperature change. Journal of Geophysical Research: Atmospheres, 113(D23): D23105, doi: 10.1029/2008JD010405
Gregory J M, Ingram W J, Palmer M A, et al. 2004. A new method for diagnosing radiative forcing and climate sensitivity. Geophysical Research Letters, 31(3): L03205
Griffies S M, Schmidt M, Herzfeld M. 2009a. Elements of mom4p1. GFDL Ocean Group Technical Report No. 6. Geophysical Fluid Dynamics Laboratory, 444. Princeton, USA.
Griffies S M, Biastoch A, Böning C, et al. 2009b. Coordinated ocean-ice reference experiments (COREs). Ocean Modelling, 26(1–2): 1–46, doi: 10.1016/j.ocemod.2008.08.007
Griffies S M, Winton M, Anderson W G, et al. 2015. Impacts on ocean heat from transient mesoscale eddies in a hierarchy of climate models. Journal of Climate, 28(3): 952–977, doi: 10.1175/JCLI-D-14-00353.1
Guan Yuping, Huang Ruixin. 2008. Stommel's box model of thermohaline circulation revisited—The role of mechanical energy supporting mixing and the wind-driven gyration. Journal of Physical Oceanography, 38(4): 909–917, doi: 10.1175/2007JPO3535.1
He J, Winton M, Vecchi G, et al. 2017. Transient climate sensitivity depends on base climate ocean circulation. Journal of Climate, 30(4): 1493–1504, doi: 10.1175/JCLI-D-16-0581.1
Held I M, Winton M, Takahashi K, et al. 2010. Probing the fast and slow components of global warming by returning abruptly to preindustrial forcing. Journal of Climate, 23(9): 2418–2427, doi: 10.1175/2009JCLI3466.1
Holland M M, Bitz C M. 2003. Polar amplification of climate change in coupled models. Climate Dynamics, 21(3–4): 221–232, doi: 10.1007/s00382-003-0332-6
Huang Ruixin. 1999. Mixing and energetics of the oceanic thermohaline circulation. Journal of Physical Oceanography, 29(4): 727–746, doi: 10.1175/1520-0485(1999)029<0727:MAEOTO>2.0.CO;2
Huang Boyin, Stone P H, Sokolov A P, et al. 2003. The deep-ocean heat uptake in transient climate change. Journal of Climate, 16(9): 1352–1363, doi: 10.1175/1520-0442-16.9.1352
Kostov Y, Armour K C, Marshall J. 2014. Impact of the Atlantic meridional overturning circulation on ocean heat storage and transient climate change. Geophysical Research Letters, 41(6): 2108–2116, doi: 10.1002/2013GL058998
Kuhlbrodt T, Gregory J M. 2012. Ocean heat uptake and its consequences for the magnitude of sea level rise and climate change. Geophysical Research Letters, 39(18): L18608
Levitus S, Antonov J I, Wang Julian, et al. 2001. Anthropogenic warming of Earth's climate system. Science, 292(5515): 267–270, doi: 10.1126/science.1058154
Lin Pengfei, Liu Hailong, Yu Yongqiang, et al. 2013. Long-term behaviors of two versions of FGOALS2 in preindustrial control simulations with implications for 20th century simulations. Advances in Atmospheric Sciences, 30(3): 577–592, doi: 10.1007/s00376-013-2186-0
Liu Hailong, Lin Pengfei, Yu Yongqiang, et al. 2012. The baseline evaluation of LASG/IAP climate system ocean model (LICOM) version 2. Acta Meteorologica Sinica, 26(3): 318–329, doi: 10.1007/s13351-012-0305-y
Meehl G A, Washington W M, Arblaster J M, et al. 2004. Factors affecting climate sensitivity in global coupled models. Journal of Climate, 17(7): 1584–1596, doi: 10.1175/1520-0442(2004)017<1584:FACSIG>2.0.CO;2
Meehl G A, Stocker T F, Collins W D, et al. 2007. Global climate projections. In: Solomon S, Qin D, Manning M, et al, eds. Climate Change 2007: The Physical Science Basis. Contribution of Working Group I to the Fourth Assessment Report of the Intergovernmental Panel on Climate Change. Cambridge: Cambridge University Press.
Munk W, Wunsch C. 1998. Abyssal recipes II: Energetics of tidal and wind mixing. Deep Sea Research Part I: Oceanographic Research Papers, 45(12): 1977–2010, doi: 10.1016/S0967-0637(98)00070-3
Randall D A, Wood R A, Bony S, et al. 2007. Climate models and their evaluation. In: Solomon S, Qin D, Manning M, et al, eds. Climate Change 2007: The physical science basis. Contribution of Working Group I to the Fourth Assessment Report of the Intergovernmental Panel on Climate Change. Cambridge: Cambridge University Press, 589–662.
Raper S C B, Gregory J M, Stouffer R J. 2002. The role of climate sensitivity and ocean heat uptake on AOGCM transient temperature response. Journal of Climate, 15(1): 124–130, doi: 10.1175/1520-0442(2002)015<0124:TROCSA>2.0.CO;2
Reintges A, Martin T, Latif M, et al. 2017. Uncertainty in twenty-first century projections of the Atlantic Meridional overturning circulation in CMIP3 and CMIP5 models. Climate Dynamics, 49(5–6): 1495–1511, doi: 10.1007/s00382-016-3180-x
Rose B E J, Armour K C, Battisti D S, et al. 2014. The dependence of transient climate sensitivity and radiative feedbacks on the spatial pattern of ocean heat uptake. Geophysical Research Letters, 41(3): 1071–1078, doi: 10.1002/2013GL058955
Rugenstein M A, Winton M, Stouffer R J, et al. 2013. Northern high-latitude heat budget decomposition and transient warming. Journal of Climate, 26(2): 609–621, doi: 10.1175/JCLI-D-11-00695.1
Schiller A, Fiedler R. 2007. Explicit tidal forcing in an ocean general

circulation model. Geophysical Research Letters, 34(3): L03611

Shen Yang, Guan Yuping. 2015. Feature of thermohaline circulation in two-layer conceptual model based on energy constraint. Science China Earth Sciences, 58(8): 1397–1403, doi: 10.1007/s11430-015-5092-8

Solomon S, Qin D, Manning M, et al. 2007. Climate Change 2007: The Physical Science Basis. Contribution of Working Group I to the Fourth Assessment Report of the Intergovernmental Panel on Climate Change. Cambridge: Cambridge University Press, 235–337

Taylor K E, Stouffer R J, Meehl G A. 2012. An overview of CMIP5 and the experiment design. Bulletin of the American Meteorological Society, 93(4): 485–498, doi: 10.1175/BAMS-D-11-00094.1

Weaver A J, Sedláček J, Eby M, et al. 2012. Stability of the Atlantic meridional overturning circulation: A model intercomparison. Geophysical Research Letters, 39(20): L20709

Winton M, Takahashi K, Held M. 2010. Importance of ocean heat uptake efficacy to transient climate change. Journal of Climate, 23(9): 2333–2344, doi: 10.1175/2009JCLI3139.1

Winton M, Adcroft A, Griffies S M, et al. 2013. Influence of ocean and atmosphere components on simulated climate sensitivities. Journal of Climate, 26(1): 231–245, doi: 10.1175/JCLI-D-12-00121.1

Winton M, Anderson W G, Delworth T L, et al. 2014. Has coarse ocean resolution biased simulations of transient climate sensitivity. Geophysical Research Letters, 41(23): 8522–8529, doi: 10.1002/2014GL061523

Yu Yi, Liu Hailong, Lan Jian. 2016. The influence of explicit tidal forcing in a climate ocean circulation model. Acta Oceanologica Sinica, 35(9): 42–50, doi: 10.1007/s13131-016-0931-9